

Observation of photonic edge states in a versatile Silicon platform

M. Hafezi,^{1,*} J. Fan,¹ A. Migdall,¹ and J. M. Taylor¹

¹*Joint Quantum Institute, National Institute of Standards and Technology / University of Maryland, College Park MD 20742*

Systems with topological order exhibit exotic phenomena associated purely with the boundaries of the system. While most systems with topological order have been electronic, advances in our understanding of synthetic gauge fields have enabled investigation of topological order in ultracold atoms or even with photons. Here, we demonstrate the experimental realization of synthetic magnetic fields for infrared photons at room temperature. Our implementation corresponds to a spin-orbit Hamiltonian, uses linear optics and does not break time reversal symmetry. As a proof of topological order, we directly observe for the first time, edge states for light in a two-dimensional system. This realization demonstrates the feasibility of using a photonic platform for the investigation of a wide range of topological order in both the non-interacting and many-body regimes and highlights the broad promise of this tool.

Particles in two-dimensional structures with a magnetic field exhibit a remarkable variety of macroscopic quantum phenomena, including integer-[1] and fractional- quantum Hall [2], quantum spin Hall effects [3], and the theoretical prediction of the emergence of particles with fractional statistics, so-called anyons [4]. Despite the great success in electronic systems, advances in the experimental efforts have been hampered by stringent experimental requirements such as purity. Recently, ultracold gases has been theoretically and experimentally under investigation for observation of these effects [5–8]. Ultracold atomic systems are advantageous since they provide tools to control various parameters of quantum Hall models. However, the atomic experimental conditions are demanding, such as achieving strong effective magnetic field. In contrast, photons, alleviating many of the previous experimental difficulties, provide a new avenue for investigation of quantum Hall physics at room temperature. More specifically, coupled optical resonator arrays provide a toolbox, in the context of quantum simulation, to engineer several classes of Hamiltonians and allow the direct observation of the wave function. Furthermore, such photonic systems provide a platform to exploit topological robustness in optical devices such as filters, switches and delay lines. For example, it has been

*Electronic address: hafezi@umd.edu

proposed that optical delay lines could be made insensitive to certain fabrication errors [9]. Here, we report the first implementation of a magnetic-like Hamiltonian in a two dimensional photonic system and present the direct observation of edge states which is the hallmark of topological orders.

Our approach is motivated by the scheme presented in Ref. [9], based on a network of coupled optical resonators. Many proposals for implementation of magnetic-like Hamiltonians in photonic systems require an external field such as large magnetic field [10, 11], strain [12], harmonic modulation [14] or optomechanical induced non-reciprocity [15]. However, it has been shown that explicitly breaking the time-reversal symmetry is not necessary [9], in direct analogy to spin-orbit interaction in electronic systems [16]. Coupled resonator systems allow direct implementation of various Hamiltonians where the entire spectrum can be probed using transport measurement, in contrast to waveguide lattice [18]. Moreover, such systems could have direct application in silicon photonics [9, 17]. Specifically, we implement a synthetic gauge potential using an induced pseudo-spin-orbit interaction where a time-reversed pair of resonator modes – clockwise and counter-clockwise circulation – acts as a pseudo-spin. Due to the relatively large size of the resonators, several tens of microns, such photonic implantation of magnetic-like Hamiltonian allows measurement of the wave function which is not readily accessible in electronic counterparts. To describe the essence of the scheme, we consider a single plaquette of our lattice which consists of four “site-resonators” and four “link-resonators” in the form of rounded rectangles, as shown in Fig. 1A. The link- and site-resonators are coupled through directional couplers to each other, and therefore, photons circulating in one direction in the site-resonators only couple with each other and with photons circulating in the opposite direction in the link-resonators. The effective length of the link-resonators is chosen to be larger than that of the site-resonators by 2η , so that the links and sites are resonant at different frequencies. Consequently, a photon resonant with the site-resonators spends substantially more time in the sites than links. We associate the clockwise photons in site-resonators with the up component of a pseudo-spin. By virtue of the time-reversal symmetry, the pseudo-spin down component (counter-clockwise photons in the site-resonators) is degenerate with the pseudo-spin up component. For the moment, we focus on the spin-up component. Depending on the positioning of the links, the photon acquires a different phase hopping forwards than backwards. In particular, the hopping process between sites 1 and 2 in Fig.1A is described by: $\hat{a}_2^\dagger \hat{a}_1 e^{-i\phi_{12}} + \hat{a}_2^\dagger \hat{a}_1 e^{i\phi_{12}}$ where \hat{a}_i is the creation operator of a photon at site i . The phase arises from an offset of the link waveguides from the symmetric point (defined as equal amounts of additional length above and below the directional coupler). Specifically, the additional phase is given by the optical length $\phi_{12} = 4\pi n x_{12}/\lambda$, where n is the index of refraction, x_{12} is the position shift of the link resonator, and λ is the wavelength of the light. Note that the additional length η and position shifts away

from the symmetric point are designed to keep the length directional couplers, the geometry of their coupling regions, and their coupling efficiencies invariant (Fig. 1A). Thus, the overall Hamiltonian describing photon hopping in the plaquette can be written:

$$- J \left[\hat{a}_2^\dagger \hat{a}_1 e^{-i\phi_{12}} + \hat{a}_3^\dagger \hat{a}_2 + \hat{a}_4^\dagger \hat{a}_3 e^{i\phi_{34}} + \hat{a}_1^\dagger \hat{a}_4 \right] + h.c.. \quad (1)$$

The photon going counter-clockwise around the plaquette acquires a $2\pi\alpha$ phase where $\alpha = 2n(x_{34} - x_{12})/\lambda$ and J is the tunneling rate. If the phase per plaquette is uniform over a region, the photonic dynamics are equivalent to those of charged particles in a uniform perpendicular magnetic field [9]. Such a system is predicted to exhibit edge states at the boundaries of that region [19, 20]. In a photonic system, such edge states can be excited by driving the system at specific frequencies.

Following that idea, to experimentally implement this approach, we fabricated a two-dimensional (2D) array of coupled optical ring resonators where the design of the waveguides in the array allows us to simulate a magnetic field for photons using the silicon-on-insulator (SOI) technology [17, 21–26]. Ring resonators were fabricated on a SOI wafer with a 220 nm thick layer of silicon on top of a 2 μm thick buried oxide (BOX) layer that isolates the optical mode and prevents it from leaking to the substrate. The cross section of the waveguides, which form the link and site resonators, was designed to be 510 nm \times 220 nm, to assure single-mode propagation of the transverse-electric (TE) light (the electric field in the slab plane) at the telecom wavelength ($\approx 1.55\mu\text{m}$). The air gap for evanescent coupling between the site-resonators and the probing waveguides (link-resonators) were chosen to be 180 nm (200 nm), respectively. The 90° bending radius of the rounded rectangles was chosen to be 6 μm to have the bending loss negligibly small [25]. The fabrication of silicon chips was performed through ePIXfab, and set-up by Leti-CEA facility. The masks were made using deep ultraviolet 193 nm photolithography and were etched in two steps of 70 nm/220 nm, for gratings/waveguides, respectively. The process was followed by thermal oxidation (10 nm) to reduce surface roughness.

In our experimental setup, grating couplers were used for input and output coupling to the device. Light scattered from the resonators was spatially imaged using a 25x microscope objective and an InGaAs infrared camera by Goodrich (640 \times 512 pixel grid with a 25 μm pitch), as shown in Fig. 1C. Such a setup allows us to measure the intensity of light from each site [27]. Transmission was measured using an optical vector analyzer (Luna technologies OVA 5000). Our photonic waveguide system consists of a 10 \times 10 lattice of site-resonators. To verify that the expected edge physics arises entirely from our synthetic gauge field, we design a phase slip between 10 \times 4 stripes. This results

in having magnetic domains that are entirely due to passive, and controlled, interference effects. The resulting edge states of the system then follow along the edge of the magnetic domains induced by this phase slip (Fig. 1B), rather than the physical edge of the system (see Supplementary Information). The effective uniform magnetic field in the stripe is given by ($\alpha \approx 0.15$). The dispersion of the system is shown in Fig. 2A, where the edge state bands are shown between magnetic bulk bands. The light is coupled to the 2D ring resonators using a bent waveguide at the two bottom corners, as shown in Fig. 1B. Depending on the pumping direction, the two different pseudo-spin components can be excited, e.g. coupling light the system at port 1 (2), pumps the system in the spin-up (spin-down) component.

As a demonstration of the scheme, we measured the transmission spectrum of the 2D system through various ports and compared it with our simulation, as shown in Fig. 2. To do this, we first characterized different system parameters using simpler devices such as a notch filter (single resonator coupled to a waveguide), and an add/drop filter (single resonator coupled to two waveguides) fabricated on the same chip to allow for calibration and characterization of the waveguides and resonators (see Supplementary Information). We estimate the probing waveguide-resonator coupling rate ($\kappa_{\text{ex}} \approx 15$ GHz), the intrinsic loss ($\kappa_{\text{in}} \approx 1$ GHz) and the tunneling rate between site-resonators ($J \approx 16$ GHz), where all measurements are within 2nm of the center wavelength of 1539 nm. Given these parameters, we simulate a 10×10 lattice using coupled mode theory (Supplementary Information), as shown in Fig. 2A. We have also considered a random onsite impurity shift of the resonance frequency with a standard deviation of $0.1J$. In a lossless system, the transmission spectrum for the spin-down (T_{12}) and spin-up (T_{34}) should be identical, although they may take different paths. However, the presence of loss breaks this symmetry. We observe a qualitative agreement between the simulation and experiment (Fig. 2B,C).

A crucial point which allows us to implement the magnetic Hamiltonian in our photonic system is the weakness of backscattering. In principle, backscattering in the waveguide and resonators can flip the pseudo-spin and destroys the desired behavior. To address this issue, we used directional couplers to reduce the effect of backscattering in the coupling regions. However, surface roughness of the waveguides still leads to some backscattering, which can accumulate in our large 2D system. Thus, the pseudo-spin can flip from up to down (i.e., clockwise to counter-clockwise) and leave the system by the opposite channel (e.g. when the system is pumped with pseudo spin up from port 1, the flipped spin exits the system at port 4). We confirm that the effect of backscattering, which is characterized by T_{14} in Figs. 2B-C, is small, as predicted previously [28].

To observe the presence of edge states in our system, we investigate the propagation of photons in the 2D system. In the presence of a magnetic field, one expects edge states to appear when the system is pumped at certain frequencies

[9]. According to the dispersion simulation (Fig. 2A), we expect the absence of bulk state and presence of edge states to occur at the frequency interval $\omega/J = 2.5 \pm .5$. Fig. 2D shows such an edge state starting at the input, routing around the 10×4 stripe edge, and leaving the system at the output. In the experiment, we observe a similar behavior, as shown in Fig. 2E. Note that compared to the simulation, the edge state in the experiment undergoes higher loss and attenuates more rapidly before getting to the other side of the 2D system. The remarkable feature of such edge states is that they route around the boundary that is defined by our synthetic magnetic field, rather than the physical edge of our system.

When the system is pumped at a different frequency, bulk states are excited which do not have a particular shape, as shown in Figs. 2F,G. It is important to note that the states propagating in the bulk are more susceptible to the frequency mismatch of the resonators, and therefore, one should not expect that the spatial profile to match the numerical simulation.

To achieve an image with high signal to noise ratio, it is necessary to reduce scattered background light. Polarizing the input light helped to reduce the background noise. Moreover, in processing the images, first the laser was tuned out of the transmission band and an image was taken. The out-of-band image was later subtracted from the in-band images, to better distinguish scattered light from the resonators and the light from background (see Supplementary Information).

We have demonstrated the presence of edge states in an engineered two-dimensional photonic system. The silicon-on-insulator technology allowed us to measure both the transport properties and the spatial wave function of such states. This platform opens the door to study different types of magnetic fields and topological orders with photons in the non-interacting regime, due to the resonant enhancement. Moreover, intriguing avenues can be seen for exploring many-body physics by integrating strong nonlinearity, such as one mediated by quantum-dots [29–32] or Rydberg atomic ensembles [33, 34].

Acknowledgments: We thank J. Chen, K. Srinivasan, S. Mittal, M. Lukin, A. Melloni, M. Fournier, G. Solomon, and E. Waks for stimulating discussions and experimental help. M.H. thanks IQOQI, Innsbruck for hospitality. This research was supported by the U.S. Army Research Office MURI award W911NF0910406, and the NSF through the Physics Frontier Center at the Joint Quantum Institute.

Disclaimer: Certain commercial equipment, instruments or materials are identified in this paper to foster

understanding. Such identification does not imply recommendation or endorsement by the National Institute of Standards and Technology, nor does it imply that the materials or equipment are necessarily the best available for the purpose.

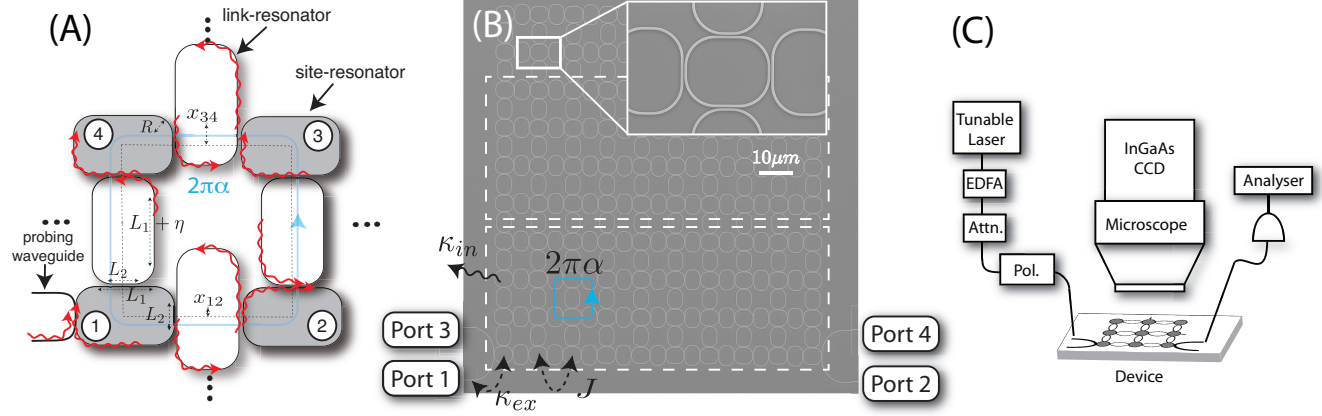


Figure 1: (A) A single plaquette consisting of 4 link resonators and 4 site resonators: gray (white) rounded rectangles represent site- (link-) resonators, respectively. The difference is due to the extra length (2η) in the link-resonators. Moreover, due to the lateral shift of the link-resonators, a photon acquires a non-zero phase when it hops between resonators (1,2) and (3,4). Therefore, a photon going counter-clockwise (clockwise) around the plaquette acquires a $2\pi\alpha$ ($-2\pi\alpha$) phase, respectively. (B) Scanning electron microscope image of the device. The stripes with uniform magnetic field are delineated with white dashed lines. (C) Schematic of the experimental setup.

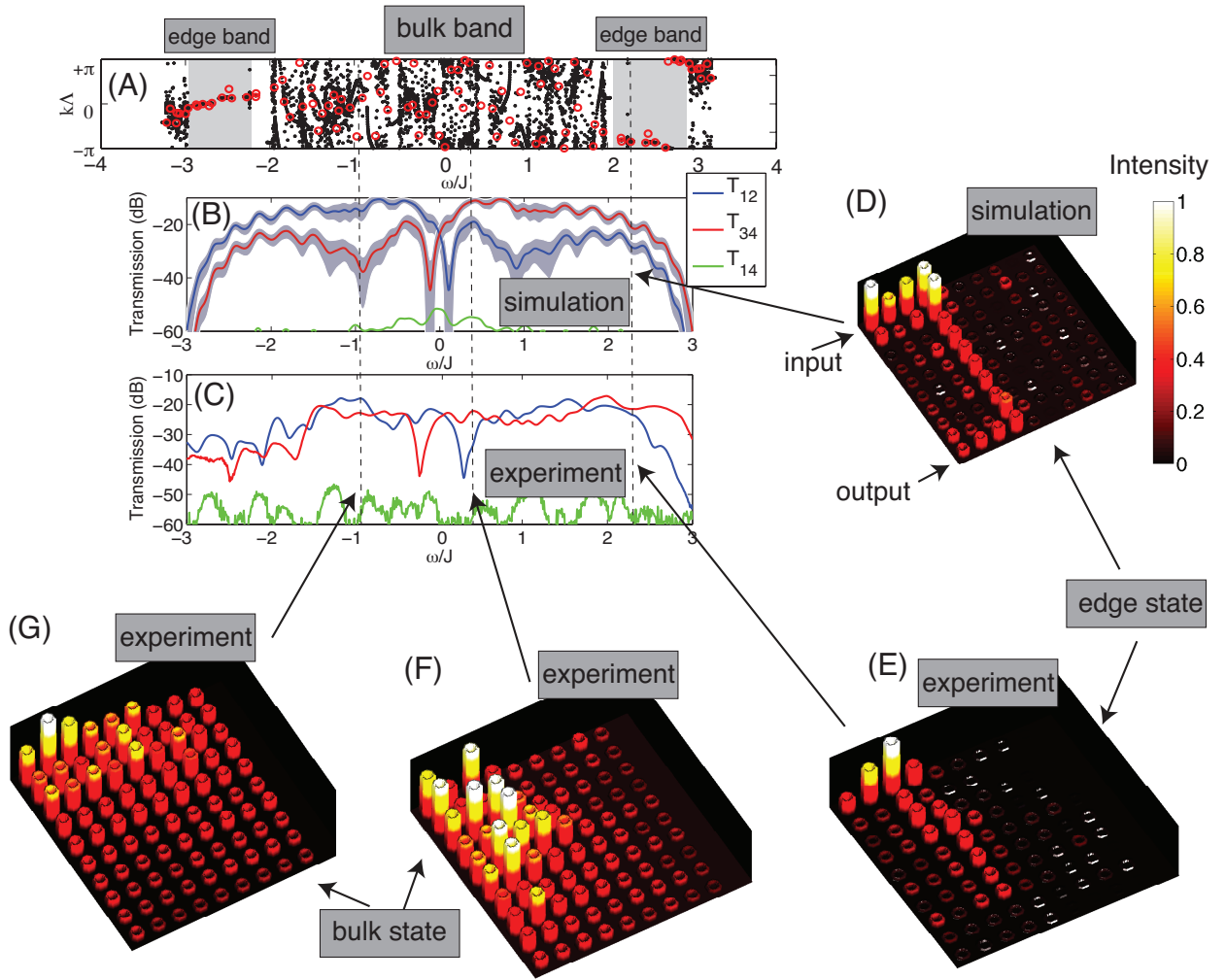


Figure 2: (A) Simulated dispersion of the system: $k\Lambda$ is the relative phase between two adjacent resonators on the edge while ω is the relative detuning of frequency with respect to the band center, in units of the tunneling rate. Red dots represent the dispersion of our system, black dots represent simulation of a longer system (10×400), to better distinguish the bulk band from the edge band. (B) Simulated transmission of a 10×10 lattice. T_{ij} is the transmittance between port i and j , as shown in Fig.1B. T_{14} measures the backscattered light. Simulation parameters are estimated from the experiment. (C) Measured transmission spectrum. (D) Simulated scattered light from a 2D array of the couple resonators, when the system is pumped at the edge state band (E) Image of the edge state; the system is pumped at the frequencies corresponding to edge state band. (F,G) Image of bulk states; the state is pumped at frequencies that are in the bulk state band. All the images are normalized to unity.

Supplementary Information

S1. Inducing a magnetic-like phase in coupled optical resonators

Here, we show that the dynamics of two ring resonators that are coupled through a middle off-resonant ring can be effectively written as two resonators coupled with a “hopping phase”. We evaluate transport properties in both cases and show that they are identical, around the resonant frequency of the side resonators.

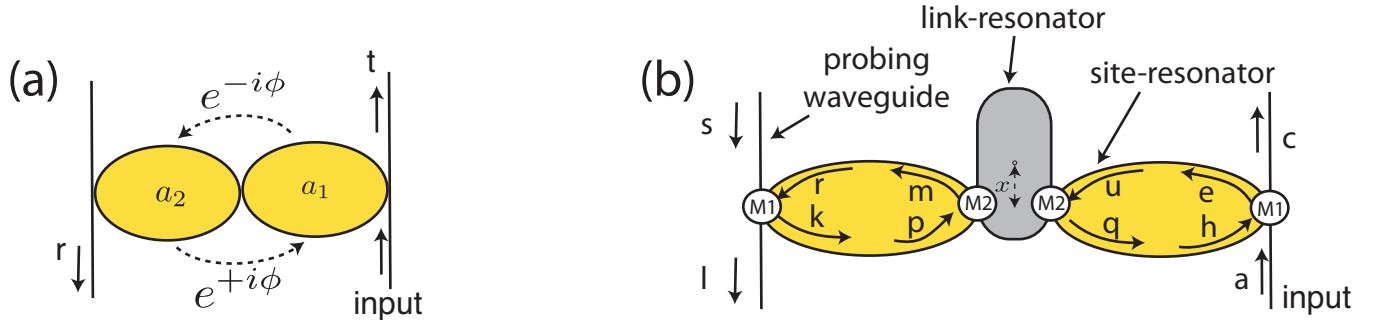


Figure 3: (a) Two ring resonator coupled with a hopping phase (ϕ) (b) Two ring resonators coupled through an off-resonant middle ring. These two systems are equivalent around the resonant frequency of side resonators.

First, we derive the transmission and reflection coefficients of two rings coupled with a hopping phase. The Hamiltonian describing such system can be written as:

$$H = -J\hat{a}_2^\dagger\hat{a}_1e^{-i\phi} - J\hat{a}_1^\dagger\hat{a}_2e^{+i\phi} \quad (2)$$

where J is the tunneling rate and ϕ is the hopping phase phase, as depicted in fig. (1a). Note that by hopping phase we mean a Hamiltonian of the kind written in Eq.(1). This should not be confused with optical non-reciprocity which requires an external field, cf. Refs. [14, 15].

We assume the resonators are single mode. Therefore, using coupled mode theory (input-output formalism), we can write the dynamics of the field inside the resonators as:

$$\frac{d}{dt} \begin{pmatrix} a_1 \\ a_2 \end{pmatrix} = \begin{pmatrix} -\kappa_{in} - \kappa_{ex} & iJe^{+i\phi} \\ iJe^{-i\phi} & -\kappa_{in} - \kappa_{ex} \end{pmatrix} \begin{pmatrix} a_1 \\ a_2 \end{pmatrix} - \sqrt{2\kappa_{ex}} \begin{pmatrix} \mathcal{E}_{in} \\ 0 \end{pmatrix} \quad (3)$$

where κ_{ex} is the coupling rate between the probing-waveguide and the side resonators and κ_{in} is the field decay rate to undesired modes. We assume a monochromatic input field at resonator one with amplitude \mathcal{E}_{in} and detuned by ω from the resonance, as shown in Fig.(1a). The output field of the resonators will be: $a_2^{out} = \sqrt{2\kappa_{ex}}a_2$, $a_1^{out} = 1 + \sqrt{2\kappa_{ex}}a_1$. Consequently, the transmission and reflection coefficients, as defined in fig. 1, are given by:

$$\begin{aligned} r_{SM} &= \frac{\sqrt{2\kappa_{ex}}a_2}{\mathcal{E}_{in}} = -\frac{2ie^{-i\phi}J\kappa_{ex}}{J^2 + (i\omega - \kappa_{ex} - \kappa_{in})^2} \\ t_{SM} &= \frac{\sqrt{2\kappa_{ex}}a_1 + 1}{\mathcal{E}_{in}} = 1 + \frac{2\kappa_{ex}(+i\omega - \kappa_{ex} - \kappa_{in})}{J^2 + (+i\omega - \kappa_{ex} - \kappa_{in})^2}. \end{aligned} \quad (4)$$

Now, we consider two ring resonators that are coupled through a middle off-resonant ring, as shown in Fig.(1b). We use the transfer matrix formalism to derive the transmission of the system. The transfer matrix for the waveguide-resonator and resonator-resonator coupling regions, respectively, are given by:

$$\begin{aligned} M_1 &= \frac{1}{t_1} \begin{pmatrix} -r_1^2 + t_1^2 & r_1 \\ -r_1 & 1 \end{pmatrix} \\ M_2 &= \frac{1}{t_2} \begin{pmatrix} -r_2^2 + t_2^2 & r_2 \\ -r_2 & 1 \end{pmatrix}. \end{aligned}$$

where t_i and r_i are the transmission and reflection coefficients of the coupling regions. Therefore, the probe waveguide-resonator coupling can be written as:

$$\begin{pmatrix} e \\ h \end{pmatrix} = M_1 \begin{pmatrix} a \\ c \end{pmatrix}, \quad \begin{pmatrix} l \\ s \end{pmatrix} = M_2 \begin{pmatrix} r \\ k \end{pmatrix}. \quad (5)$$

The input is at the right resonator, as shown Fig.(1b), so we can replace $a = 1, s = 0$. We assume that the length of the side resonators (middle resonator) are $L (L + \eta)$, so that the middle resonator becomes off-resonant with the other two. We assume the propagation constant is $\beta = 2\pi n/\lambda$, where n is the index of refraction and λ is the wavelength, and the absorption constant is α' . The free propagation inside the side resonators will be given by:

$$\begin{pmatrix} u \\ q \end{pmatrix} = \begin{pmatrix} e^{i\beta L/2 - \alpha' L/2} & 0 \\ 0 & e^{-i\beta L/2 - \alpha' L/2} \end{pmatrix} \begin{pmatrix} e \\ h \end{pmatrix}, \quad \begin{pmatrix} r \\ k \end{pmatrix} = \begin{pmatrix} e^{i\beta L/2 - \alpha' L/2} & 0 \\ 0 & e^{-i\beta L/2 - \alpha' L/2} \end{pmatrix} \begin{pmatrix} m \\ p \end{pmatrix} \quad (6)$$

and the propagation inside the middle rings is given by:

$$\begin{pmatrix} m \\ p \end{pmatrix} = M_2 \begin{pmatrix} e^{i\beta L/2 + i\beta\eta - i2\beta x - \alpha' L/2} & 0 \\ 0 & e^{-i\beta L/2 - i\beta\eta - i2\beta x - \alpha' L/2} \end{pmatrix} M_2 \begin{pmatrix} u \\ q \end{pmatrix}. \quad (7)$$

Using the above equations, we can obtain the transmission coefficients. We are interested in a limit where the coupling loss can be ignored (i.e. $|t_i|^2 + |r_i|^2 = 1$) and the junctions are highly reflective. In other words: $r_i \rightarrow \sqrt{1 - \epsilon_i^2}$, $t_i \rightarrow i\epsilon_i$, where $\epsilon_i \ll 1$. The regime of interest is near the resonant frequency of the side resonators, and is much smaller than the free spectral range (FSR), so we consider $\beta L \ll 1$. Since the propagation loss over a typical distance in our experiment is not large, we take $\alpha' L \ll 1$. Keeping terms to the total 2nd order in $\epsilon_i^2, \beta L, \alpha' L$, both in the numerator and the denominator, we find that the field in the drop channel can be simplified as:

$$r_{TM} = \frac{2e^{-i\phi} \epsilon_1^2 \epsilon_2^2}{2(2\alpha' L - 2i\beta L + \epsilon_1^2) \epsilon_2^2 \cos(\beta\eta) - i \left((2\alpha' L - 2i\beta L + \epsilon_1^2)^2 + \epsilon_2^4 \right) \sin(\beta\eta)}. \quad (8)$$

To compare this expression with the one obtained from the single-mode approximation (Eq.(4)), we use the following substitutions:

$$\epsilon_1^2 \rightarrow \frac{4\pi\kappa_{ex}}{\text{FSR}}, \quad \epsilon_2^2 \rightarrow \frac{4\pi J}{\text{FSR}}, \quad \alpha' L \rightarrow \frac{2\pi\kappa_{in}}{\text{FSR}}, \quad \beta L \rightarrow 2\pi \frac{\omega}{\text{FSR}}, \quad \beta x \rightarrow \phi \quad (9)$$

and we have

$$r_{TM} = \frac{2e^{-i\phi} J \kappa_{ex}}{2J(\kappa_{ex} + \kappa_{in} - i\omega) \cos(\beta\eta) - i(J^2 + (\kappa_{ex} + \kappa_{in} - i\omega)^2) \sin(\beta\eta)}. \quad (10)$$

We immediately see that if $\beta\eta = 3\pi/2$, this expression reduces to Eq.(4). This means that if the middle ring is anti-resonant with the side rings, the three rings can be effectively described by two resonators coupled with a hopping phase. If we have $\beta\eta = \pi/2$, the two models are again the same, only the sign of the tunneling is reversed ($J \rightarrow -J$). When the middle resonator deviates from the anti-resonant condition ($\beta\eta = \pi/2, 3\pi/2, \dots$), the system again can be effectively described by two resonators with a hopping phase, however, the effective tunneling is $J_{eff} \rightarrow J/\sin(\beta\eta)$ and system is shifted in frequency by $\omega \rightarrow \omega - J \cot(\beta\eta)$.

S2. Estimation of system parameters and numerical methods

Here we show how different system parameters can be estimated using simpler devices that we fabricated on the same chip. In particular, we consider an add/drop filter, as shown in Fig. 4. Using coupled mode theory (input-output formalism), we write the equation of motion of the resonator:

$$\dot{a} = (-\kappa_{in} - 2\kappa_{ex})a + \sqrt{2\kappa_{ex}}a_{in}(t)$$

where a_{in} is the input field and $\kappa_{ex}(\kappa_{in})$ are the extrinsic (intrinsic) decay rate of the field, respectively. Assuming that the resonator is driven by a monochromatic field with a detuning ω with respect to the resonator, we solve the system in the steady-state. Consequently, the output transmission in the drop and through channel are respectively given by:

$$R = \left| \frac{\sqrt{2\kappa_{ex}}a}{a_{in}} \right|^2 = \frac{4\kappa_{ex}^2}{\omega^2 + (2\kappa_{ex} + \kappa_{in})^2}$$

$$T = \left| \frac{a_{in} + \sqrt{2\kappa_{ex}}a}{a_{in}} \right|^2 = \frac{\omega^2 + \kappa_{in}^2}{\omega^2 + (2\kappa_{ex} + \kappa_{in})^2}.$$

Therefore, in the through port, the full width half maximum (FWHM)= $2(\kappa_{ex} + \kappa_{in})$ and the contrast is $T_{max}/T_{min} = (2\kappa_{ex} + \kappa_{in})^2/\kappa_{in}^2$. Consequently, the measured quantities for the contrast and FWHM give us both decay rate. Specifically, from the measurement we get $\kappa_{ex} = 15\text{GHz}$, $\kappa_{in} = 1\text{GHz}$. We note that the parameters change from device to device by about 15%.

We have also obtained these numbers for the notch filter, where the transmission in the single-mode approximation

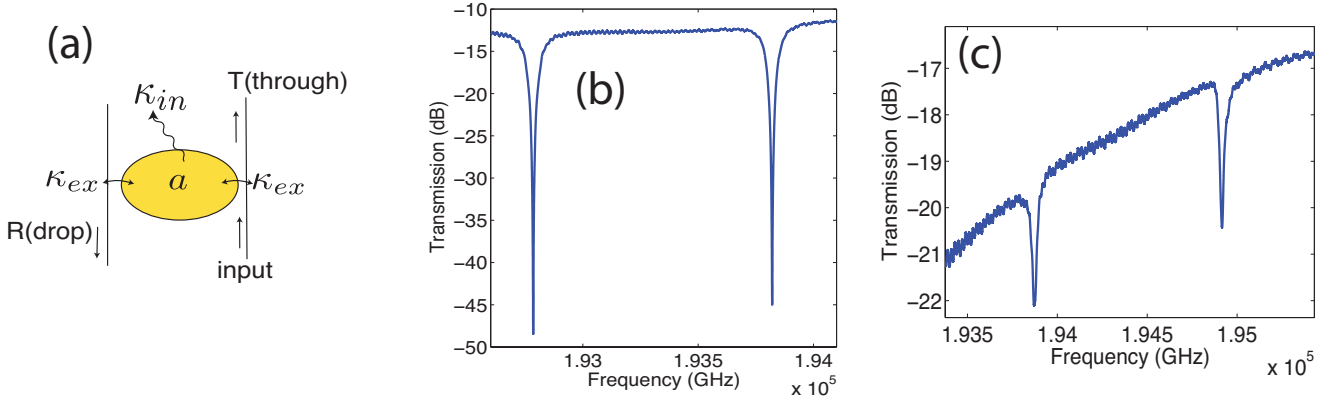


Figure 4: (a) An add/drop filter (b) Transmission spectrum in the through port for the add/drop filter (c) Transmission spectrum for a notch filter.

is given by:

$$T' = \frac{\omega^2 + (\kappa_{ex} - \kappa_{in})^2}{\omega^2 + (\kappa_{ex} + \kappa_{in})^2}. \quad (11)$$

Again the contrast and FWHM yields both the intrinsic and extrinsic decay rates $\kappa_{ex} \approx 13\text{GHz}$, $\kappa_{in} \approx 2\text{GHz}$. Note since we are operating at the over-coupled regime $\kappa_{ex} \gg \kappa_{in}$, the accuracy of the intrinsic loss is worse than that of the extrinsic loss.

For the simulation, we estimate the tunneling rate from the transmission of the 2D device, in particular, $6J \approx 95$ GHz. We used these parameters for the numerical simulation, $\kappa_{ex}/J \approx .8$, $\kappa_{in}/J \approx 0.06$. The uniform magnetic flux per plaquette is estimated to be $\alpha = 2xn/\lambda \approx .15$, in the stripes, according to our design. No direct measurement of α could be made. More precisely, we used the following gauge: for the tunneling in the y-direction we chose the phase to be zero, and for the tunneling in the x-direction, we increased the phase by α as a function of row number mod 4: zero phase for the first row, α for the second row, 2α for the third row and 3α for the fourth row, zero for the fifth row etc. This leads to a uniform flux α per plaquette in the stripes of 10×4 and a -3α phase slip in the region connecting the stripes.

In the simulation, we have considered disorder in the form of an onsite potential (i.e. frequency mismatch) with a gaussian distribution with a width $U/J = .1$. The backscattering rate in each resonator is estimated to be $\beta/J \approx 0.04$, based on the measurement of T_{14} for a single resonator. We use a generalized form of the coupled mode theory, similar to Ref. [9], to obtain various transport properties shown in fig. 2B of the main text.

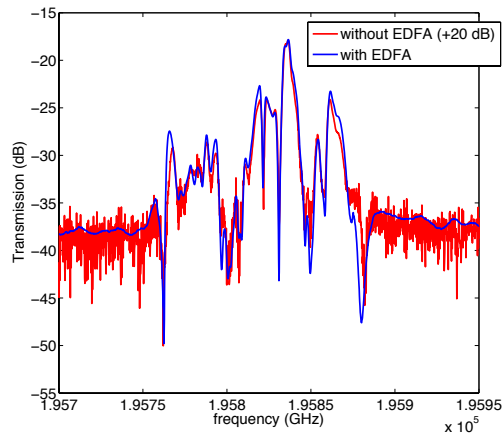


Figure 5: Transmission spectrum with and without EDFA for a 8x8 lattice

To obtain the dispersion relation (Fig. 2A in the main text), we follow Ref. [9]. We find the eigenstates of the system and calculate the dispersion relation by assigning a momentum to each eigenstate which is chosen to be the relative phase between two resonators on the edge. Since edge states are semi-one dimensional, they have a well-defined momentum while such momentum assignment to bulk states leads to random phases. The edge and bulk bands are identified in Fig. 2A of the main text. The edge states route around the stripes as shown Fig. 2D of the main text.

S3. Experimental methods and Processing

We used straight gratings (300nm spacing, 300nm linewidth, 70nm thickness) to couple light in and out of the photonic chip. The efficiency of such gratings were limited and is estimated to be roughly 8dB on each side. The fiber connections efficiency were estimated to be better than 1.5 dB. The remaining loss was due to the scattering of resonator's light out of the guided mode, which is estimated to be about 1dB per resonator. To have a significant signal to noise ratio, we amplified the LUNA OVA source light by an Erbium Doped Fiber Amplifier (EDFA) in the saturated regime with constant output power + 17dBm, as shown schematically in fig. 1C in the main text [27]. Before sending the light to the chip, the light was subject to a tunable attenuator to assure that the high intensity of the light did not lead to nonlinear response of the system. As shown in fig. 5, the amplification does not change the spectrum. Polarizer paddles were used to maximize the coupling to the TE mode of the waveguides and to increase the signal to noise ratio for the IR imaging. The contrast in the camera for the incoming photon polarization was better than 23dB.

Since the grating couplers do not have the same efficiency, we have rescaled T_{12} and T_{34} for comparison, to generate

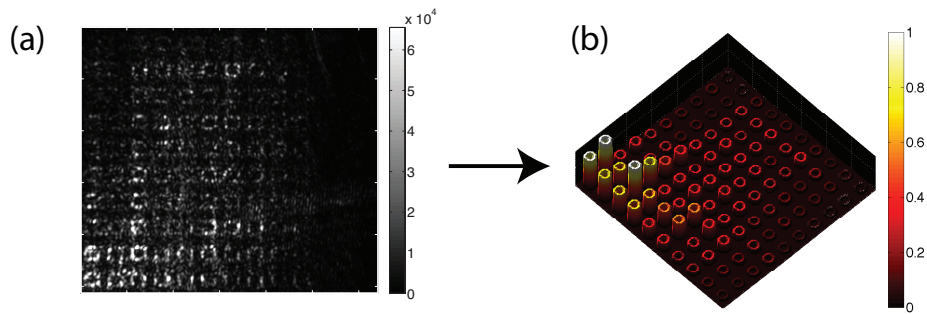


Figure 6: (a) the raw image from the camera (b) the processed image after averaging over 10x10 cells

Fig. 2B of the main text. To obtain the IR figures, such as Fig.2 E-G of the main text, we decreased the intensity of the input light to avoid saturating the camera. To reduce the effect of background light, e.g. due to scattering from the fiber holder, lens etc., and removing speckles, we used an averaging technique. More specifically, the raw image was diced into 10x10 cells so that each cell contains only one resonator and the signal was averaged over that cell (see Fig.6). The averaged intensity was then used to generate the 3D plot, where the height of each column represents the intensity of the light circulating in each resonator. We used a power-law mapping of the measured intensity for plotting. Moreover, an image was taken when the system was excited at a frequency out of the transmission band. This image was used as the background noise to be subtracted in our imaging process.

-
- [1] K. V. Klitzing and M. Pepper, *Physical Review Letters* **45**, 494 (1980).
 - [2] D. C. Tsui, H. L. Stormer, and A. C. Gossard, *Physical Review Letters* **48**, 1559 (1982).
 - [3] M. König, S. Wiedmann, C. Brüne, A. Roth, H. Buhmann, L. Molenkamp, X. Qi, and S. Zhang, *Science* **318**, 766 (2007).
 - [4] A. Comtet, T. Jolicoeur, S. Ouvry, and F. David, *The Quantum Hall Effect: Novel Excitations and Broken Symmetries*, Springer-Verlag (2000).
 - [5] N. Cooper, *Advances in Physics* **57**, 539 (2008).
 - [6] Y. Lin, K. Jimenez-Garcia and I. Spielman, *Nature* **471**, 83 (2011).
 - [7] M. Aidelsburger and M. Atala, S. Nascimbene, S. Trotzky, Y. Chen, I. Bloch, *Physical Review Letters* **107**, 255301 (2011).
 - [8] J. Dalibard and J. Gerbier, F. Juzeliunas, G. Ohberg, *Rev. Mod. Phys.* **83**, 1523 (2011).
 - [9] M. Hafezi, E. A. Demler, M. D. Lukin, and J. M. Taylor, *Nature Physics* **7**, 907 (2011).
 - [10] F. Haldane and S. Raghu, *Physical Review Letters* **100**, 13904 (2008).
 - [11] Z. Wang, Y. Chong, J. D. Joannopoulos, and M. Soljacic, *Nature* **461**, 772 (2009).
 - [12] M. C. Rechtsman, J. M. Zeuner, A. Tünnermann, S. Nolte, M. Segev, and A. Szameit, *Nature Photonics* **7**, 153 (2013).

- [13] Y. Kraus, Y. Lahini, Z. Ringel, M. Verbin, and O. Zilberberg, *Physical Review Letters* **109**, 106402 (2012).
- [14] K. Fang, Z. Yu, and S. Fan, *Nature Photonics* **6**, 782 (2012).
- [15] M. Hafezi and P. Rabl, *Optics Express* **20**, 7672 (2012).
- [16] B. Bernevig and S.-C. Zhang, *Physical Review Letters* **96**, 106802 (2006).
- [17] F. Xia, L. Sekaric, and Y. Vlasov, *Nature Photonics* **1**, 65 (2007).
- [18] D. Christodoulides, F. Lederer, and Y. Silberberg, *Nature Photonics* **424**, 817 (2003).
- [19] R. Laughlin, *Physical Review B* **23**, 5632 (1981).
- [20] B. Halperin, *Physical Review B* **25**, 2185 (1982).
- [21] B. E. Little, J. S. Foresi, G. Steinmeyer, E. R. Thoen, S. T. Chu, H. A. Haus, E. P. Ippen, L. C. Kimerling, and W. Greene, *IEEE Photonics Technology Letters* **10**, 549 (1998).
- [22] A. Melloni and M. Martinelli, *Journal of Lightwave Technology* **20**, 296 (2002).
- [23] A. Sakai, T. Fukazawa, and T. Baba, *Journal of Lightwave Technology* **22**, 520 (2004).
- [24] P. Dumon, W. Bogaerts, V. Wiaux, J. Wouters, S. Beckx, J. Van Campenhout, D. Taillaert, B. Luyssaert, P. Bienstman, D. Van Thourhout, et al., *Photonics Technology Letters, IEEE* **16**, 1328 (2004).
- [25] Y. Vlasov and S. McNab, *Optics Express* **12**, 1622 (2004).
- [26] Q. Xu, B. Schmidt, S. Pradhan, and M. Lipson, *Nature* **435**, 325 (2005).
- [27] M. Cooper, G. Gupta, J. Park, M. Schneider, I. Divliansky, and S. Mookherjea, *Optics Letters* **35**, 784 (2010).
- [28] F. Morichetti, A. Canciamilla, C. Ferrari, M. Torregiani, A. Melloni, and M. Martinelli, *Physical Review Letters* **104**, 33902 (2010).
- [29] E. Waks, K. Inoue, C. Santori, D. Fattal, J. Vuckovic, G. S. Solomon, and Y. Yamamoto, *Nature* **420**, 762 (2002).
- [30] K. Srinivasan and O. Painter, *Nature* **450**, 862 (2007).
- [31] D. Englund, A. Faraon, I. Fushman, N. Stoltz, P. Petroff, and J. Vuckovic, *Nature* **450**, 857 (2007).
- [32] I. Andrei Faraon, N. Dirk Englund, and J. Pierre Petroff, *Nature Physics* **4**, 859 (2008).
- [33] Y. O. Dudin and A. Kuzmich, *Science* **336**, 887 (2012).
- [34] T. Peyronel, O. Firstenberg, Q. Y. Liang, S. Hofferberth, A. V. Gorshkov, T. Pohl, M. D. Lukin, and V. Vuletic, *Nature* **488**, 57 (2012).